Integrated Optical Diagnostics of Cyclopentane Sprays to Characterize Transcritical Phase Transitions

M. Son[1,*], L. Zigan[1], M. Pfitzner[1], T. Sander[1]

1: Institute of Thermodynamics, Universität der Bundeswehr München, D-85577 Neubiberg, Germany
*Corresponding author: Min.Son@unibw.de

Keywords: Transcritical Spray, Phase Transition, Optical Diagnostic, Dynamic Mode Decomposition.

ABSTRACT

This research investigates spray phase transitions under subcritical and transcritical conditions relevant to high-pressure combustion systems. Using advanced optical diagnostic techniques, including shadowgraphy (SH), Mie scattering (MS), and infrared radiation (IR) measurements, the study focuses on cyclopentane sprays in a high-pressure, high-temperature chamber filled with gaseous nitrogen. Three cases are studied to understand spray behavior under varying injection conditions. SH and MS analyzes reveal significant differences across the cases. As the chamber temperature increases, the liquid core length shortens, indicating enhanced vaporization. This is particularly evident in the MS images, where step-like transitions in the axial distribution highlight abrupt phase changes from liquid to gas in subcritical conditions. Such transitions are absent under supercritical conditions, suggesting a smoother phase transition process. IR measurements provide additional insights into the spray dynamics, especially under transcritical conditions. The IR images display complex downstream (at $x/D > 125$) signal patterns with bimodal distributions. The application of inverse Abel deconvolution highlights negative intensities near the spray axis downstream, indicative of regions near the pseudo-critical temperature. This phenomenon, characterized by blocked background radiation due to critical opalescence, offers indirect evidence of the pseudo-critical temperature and the associated phase transition dynamics. Dynamic Mode Decomposition (DMD) analysis identifies dominant frequencies around 4.5 kHz, corresponding to injection pressure fluctuations. This correlation suggests that injection pressure variations significantly influence spray fluctuations. Differences in mode shapes among the cases are also observed; lateral fluctuations near the injector nozzle exit are present in Cases 1 and 2 but not in Case 3. The axial fluctuations beyond a certain length are consistent in all cases. The lateral fluctuations are related to the chamber pressure and the potential large-scale vortex formation or cavitation in the nozzle. The combined use of SH, MS, and IR methodologies provides a comprehensive understanding of transcritical spray dynamics, emphasizing the effectiveness of combining multiple optical diagnostic techniques. These findings will improve numerical simulations and contribute to the development of more efficient high-pressure combustion systems. The research underscores the complexity of phase transitions in sprays and the critical role of precise diagnostics in the advancement of combustion technology.

1. Introduction

In recent combustion engines such as internal combustion engines, gas turbine engines, and liquid rocket engines, the injection of fuel into a hot and high-pressure gas environment is common (Ma et al., 2014; Adibhatla & Kaushik, 2014; Chehroudi et al., 2002). The chamber pressure often exceeds the critical point to increase combustion efficiency, leading to phase changes and transcritical behavior (Seebald & Sojka, 2010) in the fuel spray. The phase transition of a single-component fluid generally follows its phase diagram. However, at the spray boundary, where the spray mixes with the ambient fluid, the phase change process becomes more intricate (Klima et al., 2020). The critical point of this mixture is subject to significant alterations based on the mixture ratio, which affects the phase separation at the spray interface (Zhang et al., 2022). This complex phase separation phenomenon is also evident in liquid rocket combustion, previously considered to involve mainly the mixing and burning of supercritical propellants (Traxinger, Pfitzner, et al., 2019; Traxinger, Zips, & Pfitzner, 2019).

The objective of this research is to analyze the phase transition of sprays in transcritical conditions, compared to the transition in subcritical conditions. To characterize the phase transition in transcritical conditions, three high-speed optical diagnostics were combined: focused shadowgraphy, Mie scattering, and infrared radiation measurements. The experiments were conducted in a heated high-pressure chamber with optically accessible windows. Each measurement technique complemented the others to reveal the transition characteristics. These experimental insights are poised to enhance computational fluid dynamic and molecular dynamic simulations as part of the dtec.bw project "MaST – Macro/Micro-simulation of Phase Decomposition in the Transcritical Regime."

2. Experimental setup and methods

The experimental setup included a high-pressure chamber capable of operating under a wide range of conditions, from 30 kPa to 10 MPa, with temperatures reaching up to 1000 K (Riess et al., 2018). This chamber was equipped with one sapphire window on the side facing the camera and four quartz windows on the remaining sides, each 125 mm in diameter. The injector flange was installed at the bottom of the chamber, where a single-hole gasoline research injector was mounted. The injector has a straight injection hole with a diameter of 0.2 mm and L/D of 2.55, as shown in Figure 1. Cyclopentane (C_5H_{10}) was selected as a test fuel, which was pressurized using a dual-syringe pump. The fuel temperature was controlled by heating the injector flange with a thermostat.

Three different optical diagnostic methods were used: shadowgraphy (SH), Mie scattering measurement (MS), and infrared radiation measurement (IR). SH is used to capture the spatial derivatives of light rays, which are caused by variations in refractive indices due to changes in density,

temperature, and species composition between the injected fuel and the surrounding medium. In particular, the large temperature gradients at the thick quartz glass windows in the setup could also produce Schlieren effects. Mie scattering, an elastic scattering process, occurs when the ray wavelength is shorter than the particle size, making it a reliable indicator of the presence of liquid droplets. The combination of SH and MS data is useful in distinguishing the areas where vaporization or phase transition occurs. Meanwhile, IR tracks the thermal emission from the fuel jet, which is influenced by the fuel temperature and concentration when background subtraction is applied.

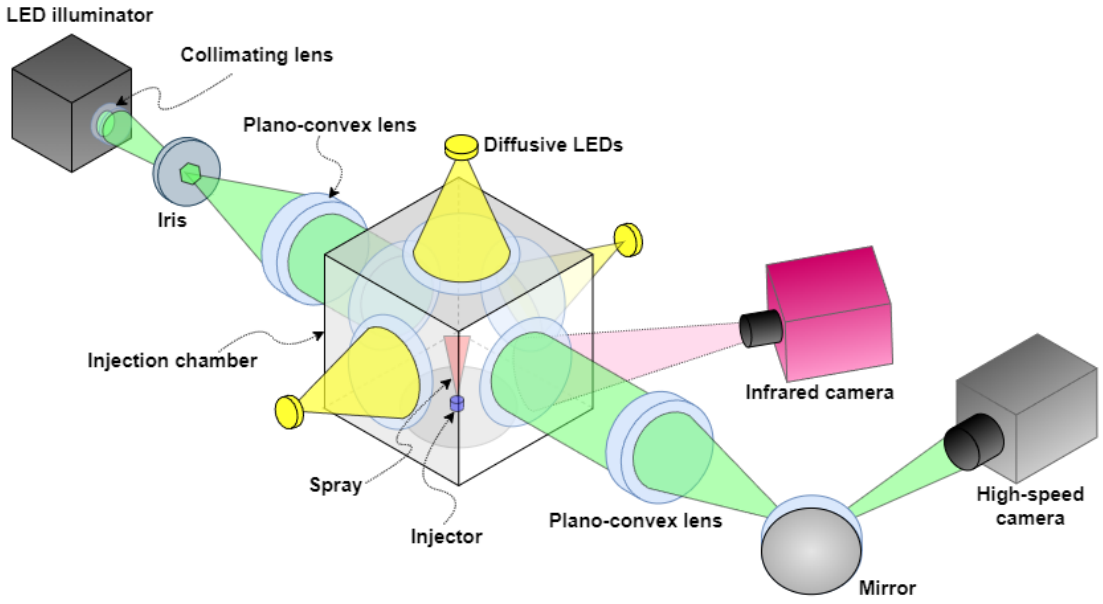

Figure 1. Experimental setup for focused shadowgraphy, Mie scattering and infrared radiation measurements.

In the experimental apparatus, as shown in Figure 1, two cameras and two light sources were utilized for the SH, MS, and IR diagnostic methods. The SH setup involved a point light from a green LED illuminator (HARDsoft IL-105G) directed towards a high-speed camera (Photron Fastcam SA-Z). For MS, three diffused LED lights were placed on the top and two side windows. Although the same high-speed camera was used to maintain a consistent field of view, simultaneous SH and MS were not feasible. Consequently, the two light sources were operated alternately. SH and MS were performed at a rate of 40,000 fps, with exposure times set at 1 µs for SH and 5 µs for MS. The IR setup used an infrared camera (TELOPS FAST M2k) with a bandpass filter (2.9-3.5 µm) to capture IR signals from cyclopentane. The camera was located at a slight angle to avoid reflections from the cooled sensor on the sapphire window, and operated at a frame rate of 4,000 fps and an exposure time of 40 µs.

To evaluate spray characteristics under varying chamber and injection conditions, three different cases were established, as detailed in Table 1 and shown in Figure 2. Case 1 remains in the liquid phase, Case 2 crosses the phase boundary to the vapor phase, and Case 3 enters the supercritical condition after injection. The pressure and temperature of the chamber are represented by P_c

and T_c, while the injection pressure and temperature are indicated by P_{inj} and T_{inj}. Furthermore, the reduced chamber pressure and temperature, $P_{r,c}$ and $T_{r,c}$, are calculated relative to the critical point of cyclopentane, which is 45.71 bar and 511.72 K, as determined by CoolProp (Bell et al., 2014). The precision of all measurements was maintained within the uncertainty of 1% (except for injection temperature, where the uncertainty was less than 0.1 K), and the data were analyzed with confidence intervals of 95%, assuming a normal distribution for the measured values (JCGM, 2008).

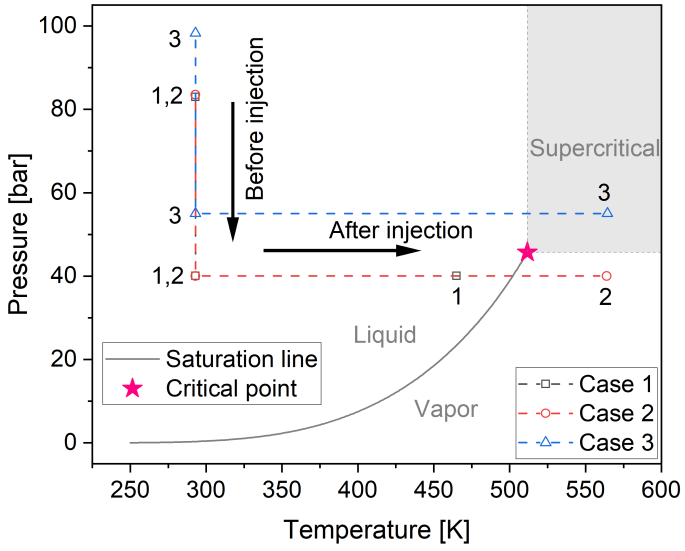

Figure 2. Phase diagram of cyclopentane.

3. Results and discussion

To compare the spray images obtained from the three diagnostic methods, 32 sets of instant spray images were averaged as a set at each frame after the start of injection, as illustrated in Figure 3. All images were normalized to an intensity range from 0 to 1, while maintaining consistent thresholds throughout the timeline. The SH images show lower intensity in the spray area compared to the other techniques because the sprays block the bright backlight, meaning that lower signal values indicate higher optical densities of the spray. In contrast, the intensities of the other methods correlate directly with the optical densities.

Table 1. Chamber and spray conditions.

Case	P_c [bar]	T_c [K]	P_{inj} [bar]	T_{inj} [K]	$P_{r,c}$	$T_{r,c}$
1	40	465	82	293	0.88	0.91
2	40	564	83	293	0.88	1.10
3	55	564	98	293	1.20	1.10

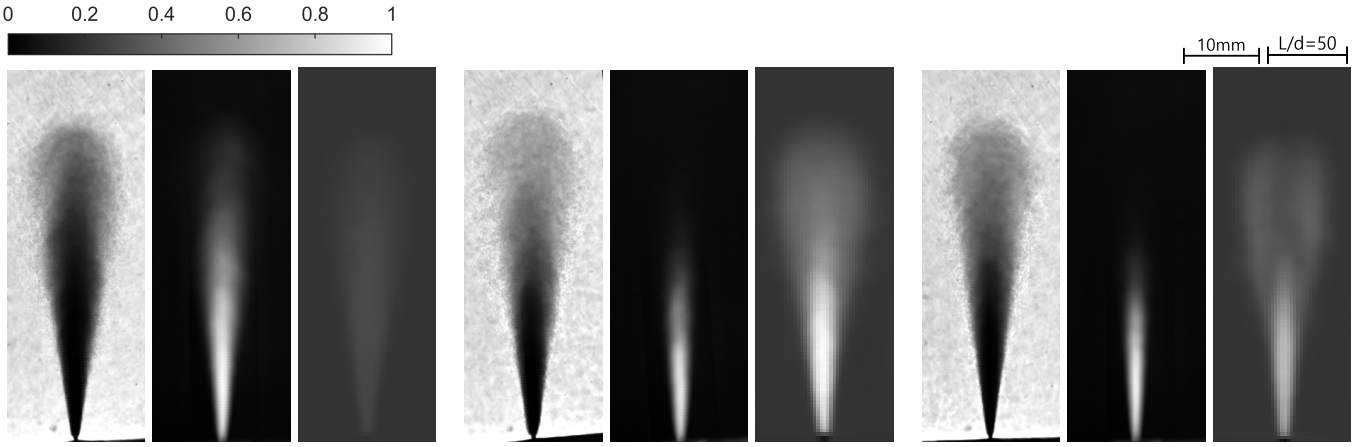

(a) Case 1 (b) Case 2 (c) Case 3

Figure 3. Normalized mean spray images of (left) shadowgraphy, (middle) Mie scattering, and (right) background-subtracted infrared radiation at t = 3.0 ms.

In SH images, the region with the lowest pixel intensity is presumed to be a dense liquid core. This is because the denser liquid phase blocks the backlight, whereas the lighter gaseous phase allows light to pass. This dense core is more prominently visible in the MS images. MS occurs when light passes through a transparent particle, such as a liquid droplet in a gas environment, leading to scattering in various directions (Wensing et al., 2016), and the MS signal directly represents the presence of the liquid phase. The strong MS signals correspond closely with the low-intensity areas in the SH images. With an increase in the chamber temperature from 465 K (Case 1) to 564 K (Case 2), the liquid core visibly shortens, as shown in the middle of Figures 3(a) and (b).

Figure 4 presents the axial distributions of image intensities along the spray center-line from three diagnostic techniques. SH signals are fully extinct near the injector, where the MS signal is strong. This indicates that the high density of the spray blocks the background light. SH intensities of Cases 2 and 3 are overall brighter than the intensity of Case 1, suggesting that the sprays of Cases 2 and 3 are less dense because of the higher chamber temperature. This trend is also shown in MS intensities as a rapid decrease in Cases 2 and 3.

The axial distributions of the MS sprays reveal some interesting results. Cases 1 and 2 have distinguishable step-like transition points, as indicated by the arrows in Figure 4, while Case 3 exhibits smooth changes. This can be explained by the different chamber conditions; the sprays of Cases 1 and 2 change phase to subcritical chamber conditions, while the spray of Case 3 undergoes transcritical changes. When the injected spray changes phase to a supercritical fluid, thermodynamic properties such as density do not suddenly change but diffuse smoothly (Carlès, 2010), and this is observed by the MS technique.

IR intensities along the axis, as shown in Figure 4, are the background-subtracted signals mainly to obtain radiation from the sprays. In addition, IR intensities are deconvoluted using the inverse

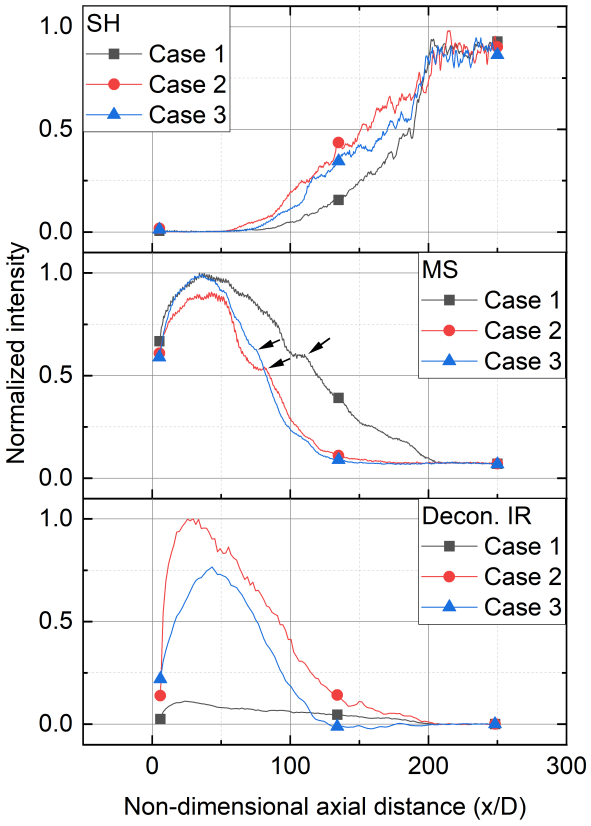

Figure 4. Axial distributions of normalized intensities from Shadowgraphy (SH), Mie scattering (MS) and background-subtracted deconvoluted infrared (Decon. IR) along the spray center-line. Arrows designate noticeable transition points.

Abel transform (Cormack, 1963) by assuming an axisymmetric spray shape because the captured IR signals are integrations of line-of-sight signals. The deconvoluted signals represent the cross-sectional IR radiation at different axial positions. The chamber temperatures in Cases 2 and 3 are around 100 K higher than in Case 1, which accounts for the noticeably low intensity of Case 1. Strong IR signals, corresponding to the dense spray region similar to MS intensities, are observed in Cases 2 and 3. This strong IR intensity near the injector region could be caused by two factors. One possibility is IR radiation scattered from the chamber heaters installed at the top, maintaining a high-temperature environment around the sprays. However, the intensity of this source is likely low. The maximum ratio of scattering to absorption occurs when the incident ray's wavelength is similar to the droplet diameter (Bohren & Huffman, 2008). However, the estimated SMDs for all cases are approximately 16 μm, ignoring the vaporization due to the short flight distance of the droplets, which are about five times larger than the filtered IR range (2.9-3.5 μm). Hence, the captured signal is supposed to primarily contain the radiation signal emitted through absorption. Consequently, the captured IR signals offer insight into the temperature and concentration of the sprays, yet quantitatively interpreting these signals remains difficult due to the varying emissivity of the spray (Golzke et al., 2016).

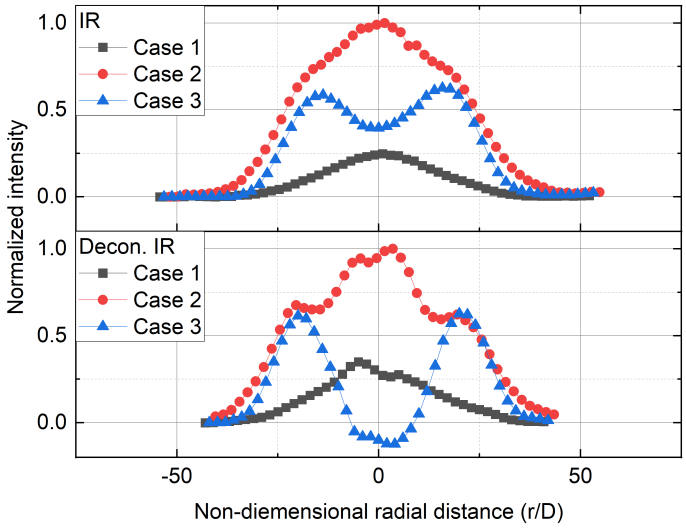

Figure 5. Radial distributions of original IR intensities (IR) and deconvoluted IR intensities (Decon. IR) at x/D = 140

Despite challenges in the quantitative analysis of the IR images, obvious negative signal distributions are observed in Case 3 downstream of the spray. This can be more clearly observed from the radial distributions at $x/D = 140$ as shown in Figure 5. In Cases 1 and 2, unimodal radial distributions are evident for the IR signals, while Case 3 presents a bimodal distribution downstream. The bimodal distribution indicates intense emission at the spray boundary, as shown in the deconvoluted intensities. Case 3 reveals bimodal peaks with negative intensities near the center of the spray. It is important to note that these negative values do not indicate negative radiation, but rather the obstruction of background radiation, since the background-subtracted results were deconvoluted. This phenomenon indicates a specific occurrence under supercritical chamber conditions (or in transcritical sprays). The spray of Case 3 experiences a phase change near the critical temperature. In this condition, critical opalescence can occur (Einstein, 1910), characterized by high scattering effects and a milky appearance (Reamer & Sage, 1957). Consequently, the transmittance in the infrared range decreases significantly during critical opalescence, and maximum opacity is observed at pseudo-critical temperature (Xing et al., 2022). This results in the spray blocking background signals, which could lead to negative values in the background-subtracted signals.

The spray angle, defined as the full cone angle measured near the injector, and the spray penetration length, defined as the furthest spray tip from the injector, were measured for each MS spray snapshot and ensemble-averaged for 32 shots, as shown in Figure 6. The MS spray angles in Cases 2 and 3 are smaller than in Case 1 because of the stronger phase change due to the higher chamber temperature. The MS spray penetration lengths clearly show the maximum lengths of the liquid core. Since the spray in Case 1 stays in the liquid phase, as shown in Figure 2, the penetration length continuously increases, while in Cases 2 and 3, it stops increasing. Interestingly, the spray angles of Cases 1 and 2 fluctuate more than in Case 3; therefore, a spectral analysis within 0.9 to

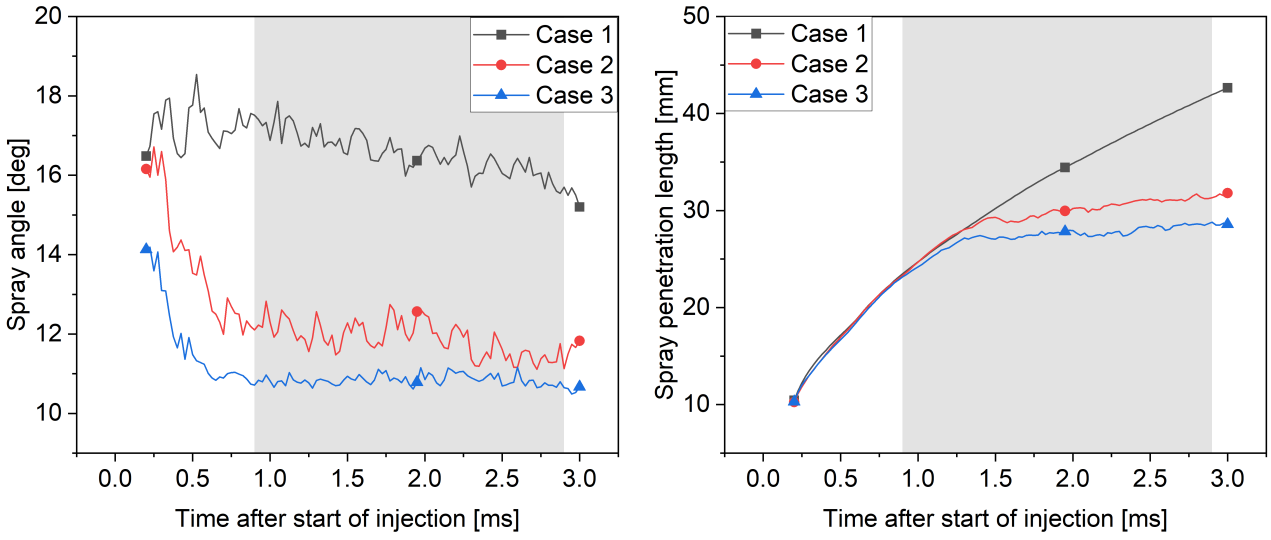

(a) (b)

Figure 6. Spray characteristics of MS over time after start of injection; (a) spray angles and (b) spray penetration lengths. The gray region from 1.9 to 2.9 ms is the data used for spectral analysis.

2.9 ms was conducted.

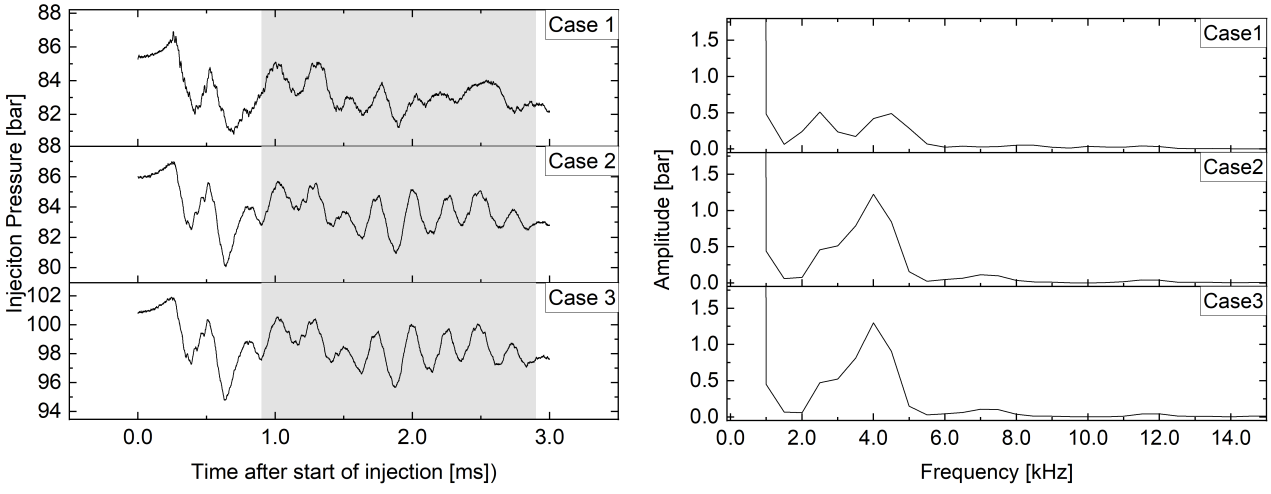

(a) (b)

Figure 7. Injection pressure characteristics; (a) injection pressure over time after start of injection and (b) FFT results. The gray region from 1.9 to 2.9 ms is the data used for spectral analysis.

To find a relation between sprays and pressure fluctuation, a fast Fourier transform (FFT) is applied to injection pressure records, as shown in Figure 7. Because the injection pressure fluctuation was much slower than the sampling rate (100 kHz) as shown in Figure 7(a), the frequency resolution was as low as 500 Hz as shown in Figure 7(b). The major peak appears in all cases at approximately 4 kHz.

Dynamic mode decomposition (DMD) is used to analyze the fluctuation of MS spray images

(Schmid, 2010; Kutz et al., 2016). In order to focus on fluctuation modes, the mean data $\bar{X}$ was subtracted from the collected data $X(t)$, and then the pure fluctuation data $X'(t)$ were used for the DMD analysis. X is a matrix of $m \times n$, where m is the number of pixels of the snapshot in a single column and n is the number of MS spray images. Taking the linear relation between the time steps n and $n+1$ as shown in Equation (1), $X'(t)$ is divided into two sets: X'_{n-1} contains the snapshots from 1 to $n-1$ and X'_n from 2 to n. A is a linear parameter.

$$X'_n = AX'_{n-1} \tag{1}$$

X'_{n-1} is decomposed by the singular value decomposition (SVD) method; $X'_{n-1} = U\Sigma V^*$. When m is larger than n, a reduced SVD can be used (Demmel, 2000), resulting in Equation (2), where Σ_r is an $n \times n$ matrix.

$$X'_{n-1} = U_r \Sigma_r V_r^* \tag{2}$$

The pseudo-inverse of X'_n can be obtained by Equation (3).

$$X'^{\dagger}_n = V_r \Sigma_r U_r^* \tag{3}$$

Then, $\tilde{A}$ can be calculated as shown in Equation (4), where $\tilde{A} = U_r^* A U_r$.

$$\tilde{A} = U_r^* X'_n V_r \Sigma_r^{-1} \tag{4}$$

The spatial mode, Φ, is calculated by Equation (5), where W are the eigenvectors and Λ are the eigenvalues in Equation (6).

$$\Phi = X'_n V_r \Sigma_r^{-1} W \tag{5}$$

$$\tilde{A}W = W\Lambda \tag{6}$$

The mode frequency in Hz, f_{DMD}, and the amplitude, b, can be calculated by Equations (7) and (8), where ν is the frame rate of the images and $\Phi^{\dagger}$ is the pseudo-inverse of Φ.

$$f_{DMD} = \frac{|\nu\Omega|}{2\pi} \tag{7}$$

$$b = \Phi^{\dagger} X'(1) \tag{8}$$

$$K = \frac{P_i n - P_v}{P_i n j - P_c} \tag{9}$$

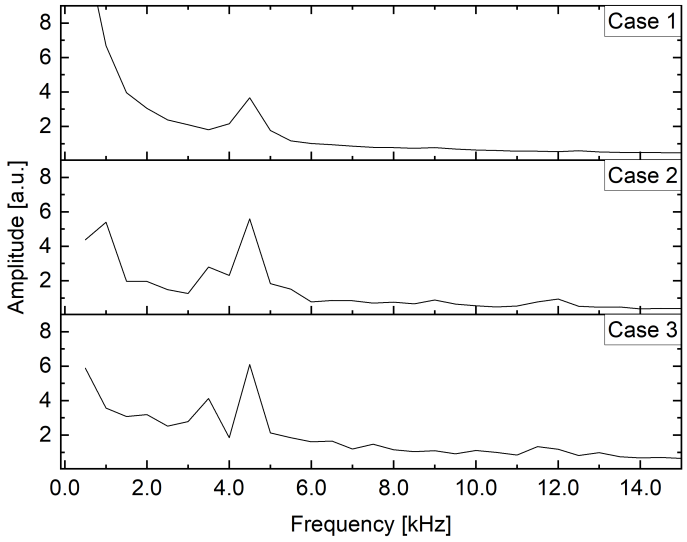

Figure 8. DMD mode amplitudes.

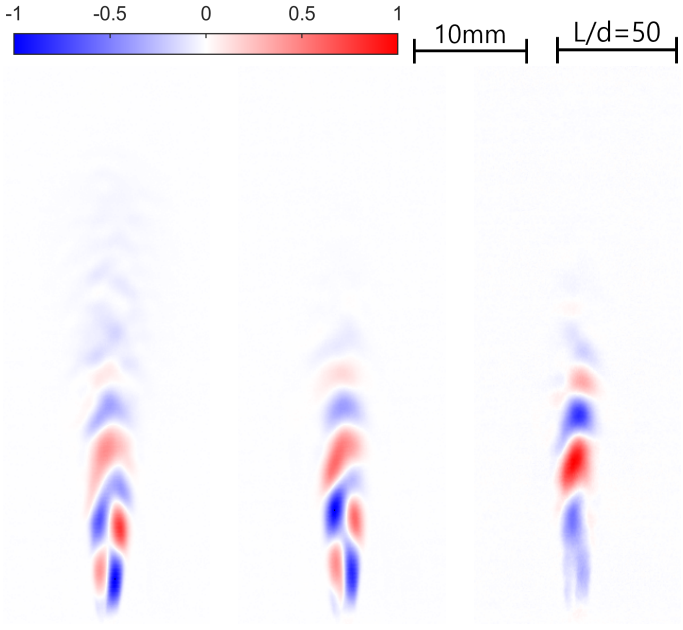

(a) Case 1 (b) Case 2 (c) Case 3

Figure 9. DMD spatial modes at 4.5 kHz.

From the DMD analysis, the dominant frequencies of all cases appear at 4.5 kHz as shown in Figure 8. Because these peaks are similar to the peaks of the injection pressures, the spray fluctuation can potentially be caused by the injection pressure fluctuation. Although the peak frequencies are similar in all cases, the mode shapes have some differences as shown in Figure 9. Cases 1 and 2 have lateral fluctuations near the nozzle, while Case 3 has no lateral mode. After a specific length, the sprays fluctuate in the axial direction in all cases. The lateral fluctuation is related to the chamber pressure, which can potentially induce cavitation or large-scale turbulences inside the nozzle.

The cavitation number, K, is defined by Equation (9), where P_v is the saturation pressure of cyclopentane at 293 K. When K decreases, the chance of cavitation increases, and there is a critical cavitation number when the cavitation starts. K is 1.94 for Cases 1 and 2, and 2.3 for Case 3. Because the critical K for the diesel injector is known to be 1.6 (Payri et al., 2013), the K in this study is in the range of non-cavitating flow. However, another study reported that cavitation can occur when K is less than 2 (Son et al., 2023).

4. Conclusions

This research focused on investigating spray phase transitions under subcritical and transcritical conditions relevant to high-pressure combustion systems. Using optical diagnostic techniques such as shadowgraphy (SH), Mie scattering (MS), and infrared radiation (IR) measurements, the study analyzed cyclopentane sprays in a specially equipped high-pressure and high-temperature spray chamber filled with gaseous nitrogen. Three distinct cases were explored to examine spray behaviors under varying subcritical and transcritical injection conditions.

The findings of the SH and MS analyzes were consistent, revealing differences between cases. A notable observation was the shortening of the liquid core length with an increase in chamber temperature, as evident in the MS images. Particularly in subcritical conditions, the MS images displayed distinct step-like transitions in axial distribution, signifying abrupt changes from liquid to gas phases, a phenomenon absent in supercritical chamber conditions. The IR images offered additional insight, especially under transcritical conditions. These images presented complex downstream signal patterns, with bimodal distributions being a prominent feature. Through the application of inverse Abel deconvolution, the analysis highlighted negative intensities near the spray axis downstream. This region, characterized by blocked background radiation due to critical opalescence, can provide indirect evidence of the pseudo-critical temperature.

Dynamic mode decomposition (DMD) analysis revealed that the dominant frequencies of spray fluctuations, around 4.5 kHz, are similar to those observed in injection pressure fluctuations, suggesting a causal relationship. Differences in mode shapes were observed among cases, with lateral fluctuations near the nozzle in Cases 1 and 2 but not in Case 3. These lateral fluctuations were associated with chamber pressure, which could induce cavitation within the nozzle.

The combined use of SH, MS, and IR methodologies yielded a comprehensive understanding of transcritical spray dynamics, emphasizing the effectiveness of combining multiple optical diagnostic techniques to reveal complex phase transitions in high-pressure combustion environments. The results of this study will support numerical simulations to study detailed spray behaviors in the future.

Acknowledgements

This research is funded by dtec.bw — Digitalization and Technology Research Center of the Bundeswehr under the project MaST – Macro/Micro-simulation of Phase Decomposition in the Transcritical Regime. dtec.bw is funded by the European Union — NextGenerationEU. The authors thank the group Professur für Fluidsystemtechnik (FST), Friedrich – Alexander Universität Erlangen – Nürnberg (FAU), and Telops Inc. for support of the experiments. Michael Pfitzner thanks ITIS e.V. for supporting his work.

Nomenclature

A	Linear parameter matrix [-]
b	Amplitude of the mode [-]
f_{DMD}	DMD mode frequency [Hz]
K	Cavitation number [-]
P_c	Chamber pressure [Pa]
P_{inj}	Injection pressure [Pa]
P_r, c	Reduced chamber pressure [-]
P_v	Saturation pressure [Pa]
T_c	Chamber temperature [K]
T_{inj}	Injection temperature [K]
T_r, c	Reduced chamber temperature [-]
U	Left singular vectors matrix [-]
V	Right singular vectors matrix [-]
W	Eigenvectors matrix [-]
X	Matrix of snapshot data [-]
$\bar{X}$	Mean data matrix [-]
$X'(t)$	Pure fluctuation data [-]
ν	Frame rate of the images [Hz]
Φ	Spatial mode matrix [-]
Σ	Singular values matrix [-]
Λ	Eigenvalues matrix [-]

References

Adibhatla, S., & Kaushik, S. (2014). Energy and exergy analysis of a super critical thermal power

plant at various load conditions under constant and pure sliding pressure operation. *Applied thermal engineering*, *73*(1), 51–65.

Bell, I. H., Wronski, J., Quoilin, S., & Lemort, V. (2014). Pure and pseudo-pure fluid thermophysical property evaluation and the open-source thermophysical property library coolprop. *Industrial & engineering chemistry research*, *53*(6), 2498–2508.

Bohren, C. F., & Huffman, D. R. (2008). *Absorption and scattering of light by small particles*. John Wiley & Sons.

Carlès, P. (2010). A brief review of the thermophysical properties of supercritical fluids. *The Journal of Supercritical Fluids*, *53*(1-3), 2–11.

Chehroudi, B., Cohn, R., & Talley, D. (2002). Cryogenic shear layers: Experiments and initial growth rates of round cryogenic jets at subcritical and supercritical pressures. *International Journal of Heat and Fluid Flow*, *23*(5), 554–563.

Cormack, A. M. (1963). Representation of a function by its line integrals, with some radiological applications. *Journal of applied physics*, *34*(9), 2722–2727.

Demmel, J. (2000). Singular value decomposition. In *Templates for the solution of algebraic eigenvalue problems: A practical guide* (pp. 135–147). SIAM.

Einstein, A. (1910). Theorie der opaleszenz von homogenen flüssigkeiten und flüssigkeitsgemischen in der nähe des kritischen zustandes. *Annalen der Physik*, *338*(16), 1275–1298.

Golzke, H., Leick, P., & Dreizler, A. (2016). Differential infrared thermography of gasoline direct injection sprays. *Quantitative InfraRed Thermography Journal*, *13*(1), 50–69.

JCGM. (2008). Evaluation of measurement data—guide to the expression of uncertainty in measurement. *Int. Organ. Stand. Geneva ISBN*, *50*, 134.

Klima, T. C., Peter, A., Riess, S., Wensing, M., & Braeuer, A. S. (2020). Quantification of mixture composition, liquid-phase fraction and-temperature in transcritical sprays. *The Journal of Supercritical Fluids*, *159*, 104777.

Kutz, J. N., Brunton, S. L., Brunton, B. W., & Proctor, J. L. (2016). *Dynamic mode decomposition: data-driven modeling of complex systems*. SIAM.

Ma, P., Bravo, L., & Ihme, M. (2014). Supercritical and transcritical real-fluid mixing in diesel engine applications. In *Proceedings of the summer program, center for turbulence research, stanford university* (pp. 99–108).

Payri, R., Salvador, F., Gimeno, J., & Venegas, O. (2013). Study of cavitation phenomenon using different fuels in a transparent nozzle by hydraulic characterization and visualization. *Experimental Thermal and Fluid Science*, *44*, 235–244.

Reamer, H., & Sage, B. (1957). Demonstration of critical phenomena for pure substances and mixtures. *American Journal of Physics*, *25*(2), 58–63.

Riess, S., Weiss, L., Peter, A., Rezaei, J., & Wensing, M. (2018). Air entrainment and mixture distribution in diesel sprays investigated by optical measurement techniques. *International Journal of Engine Research*, *19*(1), 120–133.

Schmid, P. J. (2010). Dynamic mode decomposition of numerical and experimental data. *Journal of fluid mechanics*, *656*, 5–28.

Seebald, P., & Sojka, P. (2010). Supercritical and transcritical injection. In *Handbook of atomization and sprays: Theory and applications* (pp. 255–261). Springer.

Son, M., Börner, M., Armbruster, W., & Hardi, J. S. (2023). Orifice flow dynamics in a rocket injector as an excitation source of injector-driven combustion instabilities. *Aerospace*, *10*(5), 452.

Traxinger, C., Pfitzner, M., Baab, S., Lamanna, G., & Weigand, B. (2019). Experimental and numerical investigation of phase separation due to multicomponent mixing at high-pressure conditions. *Physical Review Fluids*, *4*(7), 074303.

Traxinger, C., Zips, J., & Pfitzner, M. (2019). Single-phase instability in non-premixed flames under liquid rocket engine relevant conditions. *Journal of Propulsion and Power*, *35*(4), 675–689.

Wensing, M., Vogel, T., & Götz, G. (2016). Transition of diesel spray to a supercritical state under engine conditions. *International Journal of Engine Research*, *17*(1), 108–119.

Xing, K., Ji, Y., Wang, Z., Wang, M., Liu, Y., Xu, H., & Xiao, G. (2022). A potentially non-contact monitor method for co2 at the pseudo-critical region using infrared spectrometer. *Journal of CO2 Utilization*, *56*, 101842.

Zhang, H., Yi, P., & Yang, S. (2022). Multicomponent effects on the supercritical co2 systems: Mixture critical point and phase separation. *Flow, Turbulence and Combustion*, *109*(2), 515–543.